PCCP

RSC Publishing

PAPER

View Article Online
View Journal | View Issue

Cite this: *Phys. Chem. Chem. Phys.*, 2013, **15**, 20641

Glassy dynamics and physical aging in fucose saccharides as studied by infrared- and broadband dielectric spectroscopy

Wilhelm Kossack,*[a] Karolina Adrjanowicz,[bc] Magdalena Tarnacka,[b] Wycliffe Kiprop Kipnusu,[a] Mateusz Dulski,[b] Emmanuel Urandu Mapesa,[a] Kamil Kaminski,[ab] Sebastian Pawlus,[b] Marian Paluch[b] and Friedrich Kremer[a]

Received 19th June 2013,
Accepted 15th October 2013

DOI: 10.1039/c3cp52551a

www.rsc.org/pccp

Fourier Transform Infra Red (FTIR) and Broadband Dielectric Spectroscopy (BDS) are combined to study both the intra- and inter-molecular dynamics of two isomers of glass forming fucose, far below and above the calorimetric glass transition temperature, T_g. It is shown that the various IR-active vibrations exhibit in their spectral position and oscillator strength quite different temperature dependencies, proving their specific signature in the course of densification and glass formation. The coupling between intra- and inter molecular dynamics is exemplified by distinct changes in IR active ring vibrations far above the calorimetric glass transition temperature at about $1.16T_g$, where the dynamic glass transition (α relaxation) and the secondary β relaxation merge. For physically annealed samples it is demonstrated that upon aging the different moieties show characteristic features as well, proving the necessity of atomistic descriptions beyond coarse-grained models.

1 Introduction

The dynamic glass transition (DGT) is one of the most investigated phenomena in condensed matter physics,[1–5] and its underlying mechanism is still a matter of hot debate. This is reflected in the large number of experimental studies on this issue, *e.g.* by dynamical mechanical thermal analysis, nuclear magnetic resonance (NMR), temperature modulated, as well as usual differential scanning calorimetry, light or particle scattering, photon correlation spectroscopy and many more.[6–9] Furthermore, there is a multitude of different, controversially discussed models, such as the Adam–Gibbs model with its cooperatively rearranging regions, free volume theory, mode coupling theory, as well as the random first order transition or the two order parameter model.[10–13] All these models rely on different assumptions concerning the inter-molecular interactions, but none takes into account the intra-molecular interactions and how these may depend on molecular structure and temperature. But, recent NMR-studies reveal changes in the intra-molecular mobility in the course of vitrification.[14–16] The importance of this mobility in the sense of (sub-) molecularly specific contributions to the DGT has been recently proven by a combination of Broadband Dielectric Spectroscopy (BDS) and Fourier Transform Infrared Spectroscopy (FTIR).[17–19] This combined approach, measuring the inter- and intra-molecular interactions by the two respective techniques, is utilized here to study the glass formation of two isomeric forms of fucose, a saccharide with pharmaceutical applications.[20] Both methods (for a review see the monographs of Kremer and Schönhals[21] and Griffiths and Haseth[22]) have been used separately before to investigate similar glass forming sugars of different molecular weights. Changes in temperature (T), pressure, chemical structure and purity have been studied by BDS by several authors revealing a strong impact of all four on the emerging dynamics.[23–31] Using FTIR Imamura *et al.*[32] and Wolkers *et al.*[33,34] found a remarkable sensitivity to the glass transition of the spectral positions of hydroxyl group vibrations. In the following we present the temperature dependence of fucose in a wide range around the glass transition temperature, T_g, and time dependent (aging) measurements for $T < T_g$. Insights into the molecular scale are gained by analysis of FTIR active vibrations of all molecular moieties and detailed comparison with the dynamic properties obtained by BDS.

2 Experimental

The chemical structure of D- and L-fucose is presented in Fig. 1, including assignments of FTIR bands as well as dielectric α, β and γ relaxations. Both samples are supplied by Sigma Aldrich

[a] *Institute of Experimental Physics, University of Leipzig, Linnestr. 5, 04103 Leipzig, Germany. E-mail: wilhelm.kossack@physik.uni-leipzig.de*
[b] *Institute of Physics, University of Silesia, ul. Uniwersytecka 4, 40-007 Katowice, Poland*
[c] *NanoBioMedical Centre, Adam Mickiewicz University, ul. Umultowska 85, 61-614 Poznan, Poland*

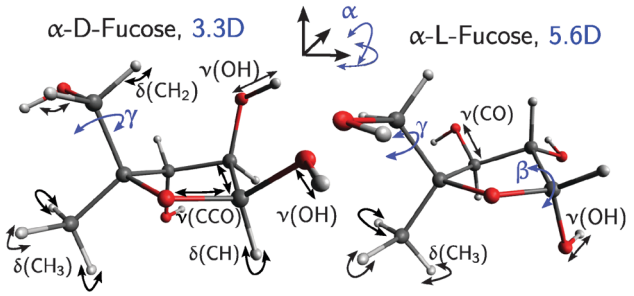

Fig. 1 Chemical structure of L- and D-fucose in α-fucofuranose form; the dielectric relaxations (dynamic glass transition (α relaxation), secondary β and γ relaxations) and IR active vibrational modes are indicated as well as the overall dipole moment. Oxygen, carbon and hydrogen atoms are di in red, grey and light grey, respectively.

with purity higher than 99% in an anhydrous, crystalline state. The samples are first melted at $T = 418$ K between stainless steel electrodes before dielectric measurements are performed starting from $T = 335$ K to $T = 143$ K in steps of 4 K and at frequencies ranging from $10^2 < f < 10^7$ Hz by employing a Novocontrol Alpha analyzer accomplished with a Quatro temperature controller (temperature stability: 0.1 K). Samples for FTIR measurements are prepared in the same manner as described above but kept between KBr windows instead of metal electrodes. IR spectra are collected at each 2 K between $T = 393$ K and 253 K in the range of 700 to 6000 cm^{-1} and a spectral resolution of 2 cm^{-1} using a Bio-Rad FTS-6000 spectrometer. The temperature is controlled using a Linkam THMS 600 heating stage with an accuracy of about 0.2 K and a net heating rate of about 1.4 K min^{-1}. No indications of thermal or chemical degradation (caramelization) are observed in the FTIR spectra collected upon melting of D- and L-fucose, nor are any changes in colour observable. For time dependent (aging) experiments the same experimental setups and samples are used. To allow observation of large effects during physical aging, we equilibrate the samples at 418 K for about 5 min and cool them afterwards at a rate of 33 K min^{-1} (FTIR) or 10 K min^{-1} (BDS) to the designated temperature before starting the measurements. BDS experiments are performed at $T = 273$ K, 278 K and 283 K where the β and γ processes are in the accessible frequency range. Effects of aging that can be seen with FTIR are subtle and, therefore, we chose aging temperatures closer to T_g, where the effects are more pronounced (eight measurements in between 287 and 300 K and just one at 273 K).

By use of the Gaussian[35] and the orca[36] software package the geometry of all forms† of fucose is optimized in the gas phase using density functional theory (DFT)[37–39] with Becke's hybrid exchange, correlated three-parameter- and the Lee–Yang–Parr correlation functional (B3LYP)[40–42] utilizing standard basis sets: 6-311++G(2d,2p).[42,43] Afterwards the dipole moments (Fig. 1) and normal modes are calculated, according to which we assign the observed absorption bands to molecular vibrations (Table 1).

† α- and β-fucose in furanose as well as pyranose forms for the D- and L-stereoisomers' chair and boat conformations.

3 Results and discussion

3.1 Analysis of spectra

Dielectric measurements above T_g reveal a broad intense relaxation process, the dynamic glass transition (α relaxation), that shifts to lower frequencies upon decreasing temperature. At the calorimetric glass transition temperature the relaxation time is typically 100 s (Fig. 2). Additionally at these elevated temperatures a significant contribution due to dc conductivity is found as in many other carbohydrates. This is due to the proton conduction, as shown by Crofton and Pethrick[44] and later on by Kaminski *et al.*[45] Within the glassy state the time scale of structural relaxation exceeds the experimental frequency window. Instead, two secondary dielectric relaxation processes become accessible, labelled for our purpose as β and γ (Fig. 2a and b). This is a common scenario for monosaccharides such as D-glucose, fructose, galactose and L-sorbose.[46] There are different views concerning the molecular origin of the slower relaxation mode (β). Authors discussed it as the genuine Johari–Goldstein relaxation of saccharides, relying on the pressure sensitivity of this mode.[46] But this process may also originate from the conversion between different conformations of the saccharide ring, whose existence has been proven by NMR, in particular there exist boat (B), half chair (H) and skew (S) conformations.[47] The faster (γ) relaxation processes result from motions of the hydroxymethylene (CH_2OH, Fig. 1) units as discussed earlier in the literature.[23] Comparing the BDS spectra of the two samples we find large dielectric strengths for L-fucose compared to the D form for all dielectric relaxations (Fig. 3b). This is attributed to the different overall dipole moment as discussed later on. But, apart from that no significant differences are observed in the BDS data.

To monitor intra-molecular interactions, FTIR measurements of D- and L-fucose are performed above and below the calorimetric glass transition temperature (Fig. 2c and d). Because of mutarotation, different isomers are present in the sample with their respective concentrations depending on temperature.[26,48,49] Consequently, the IR spectrum of each tautomer of D- and L-fucose, that can be formed during this chemical reaction, is calculated. It turns out that some of the bands are specific for some tautomers, whereas others originate from vibrations common to all isomeric species (Table 1). Upon lowering temperature the spectral positions, ν_{max}, and oscillator strengths, f_{ij}, of the bands change characteristically. Similar to the dielectric measurements, we observe only slight deviations between L- and D-fucose, particularly in the oscillator strengths of absorption bands at around 870 and 920 cm^{-1} (Fig. 2d). This appears to be reasonable, as these bands have contributions from stretching vibrations of C–OH groups, whose dipolar character is influenced by the orientation of the chiral centre, if closely attached to it (compare Table 1 and Fig. 1).

3.2 Molecular dynamics

By fitting Havriliak Negami functions[50] to the loss spectra of both fucoses, relaxation times, τ, as well as dielectric strengths, $\Delta\varepsilon$, of the α, β and γ relaxations are determined for all temperatures. The structural relaxation times (τ_α, *cf.* Fig. 3a)

Table 1 Molecular assignments and abbreviation of bands observed in FTIR spectra presented in Fig. 1; ν: stretching, δ: deformation, R refers to the sugar ring

ν_{max}/cm^{-1}	Abbrev.	α-L-Fucopyranose	α-L-Fucofuranose	β-L-Fucopyranose	β-L-Fucofuranose
811	$\delta\nu_3$(R)	ν(CCO), δ(CH)			
856	ν(CC)			ν(CC), δ(CH)	
876	δ(CC)	δ(CH), $\delta(CH_3)$, δ(OH)			
900	$\delta\nu_1$(R)		$\delta(CH_2)$, $\delta(CH_3)$, δ(OH)	$\delta(CH_2)$, $\delta(CH_3)$, ν(R)	$\delta(CH_2)$, $\delta(CH_3)$, ν(R)
905	$\delta\nu_2$(R)	ν(R), $\delta(CH_3)$, δ(CH)			$\delta(CH_2)$, $\delta(CH_3)$, ν(R)
945	δ(CH)			δ(CH), $\delta(CH_3)$	
964	δ_2(CH)	δ(CH), δ(R), $\delta(CH_3)$			δ(R), δ(CH), $\delta(CH_3)$
1170	$\nu(CCH_3)$	ν(CCO), ν(R), ν(C–CH_3)		ν(CCO), ν(R), ν(C–CH_3)	ν(CCO), ν(R), ν(C–CH_3)
3400	ν(OH)	ν(OH) H-bonded	ν(OH) H-bonded	ν(OH) H-bonded	ν(OH) H-bonded

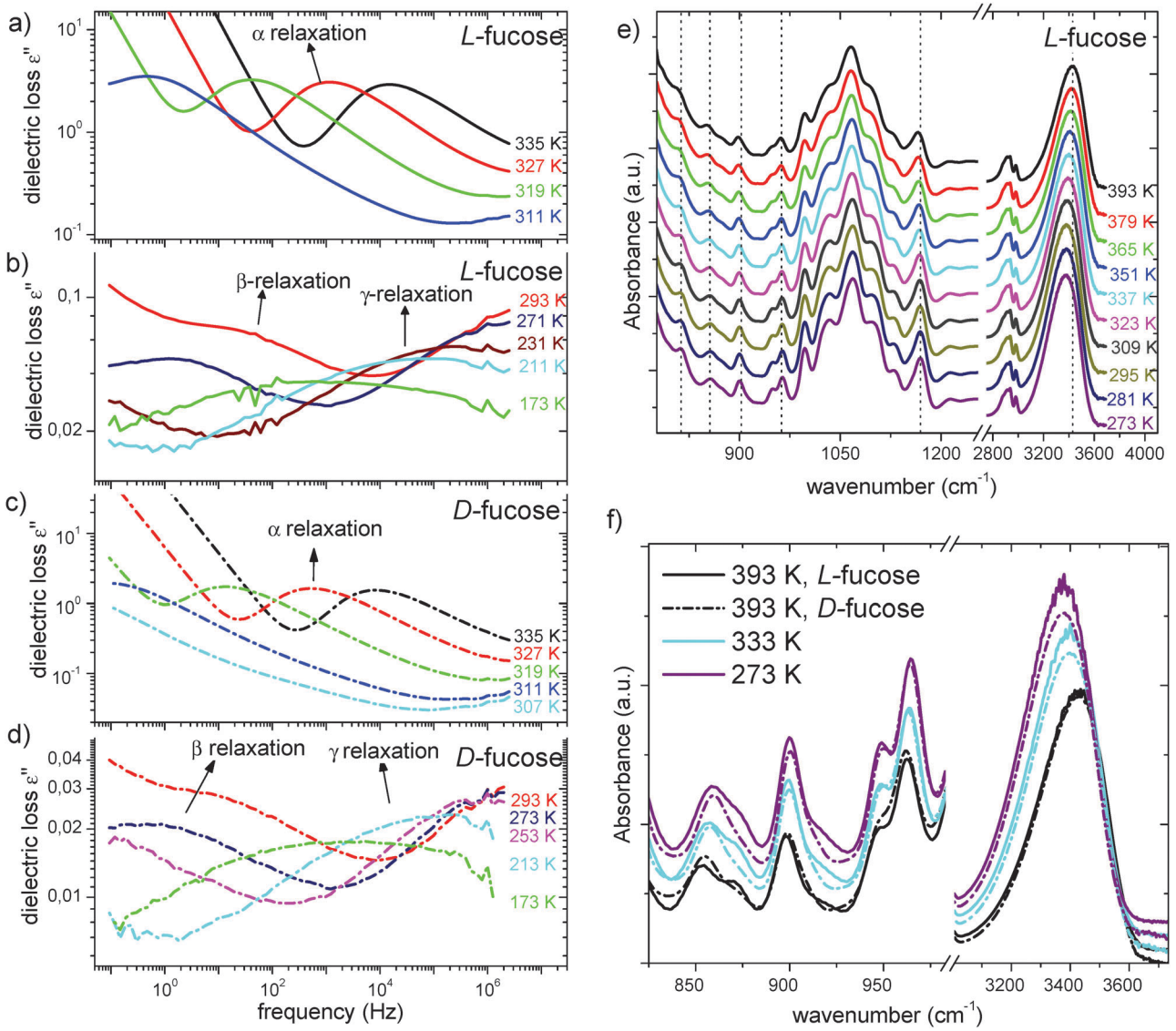

Fig. 2 Dielectric loss spectra of L- (a, b) and D-fucose (c, d) measured above and below T_g; (e) FTIR spectra of L-fucose at different temperatures as indicated by colour; vertical dashed lines are a guide for the eye. (f) FTIR spectra at selected temperatures of the L and D form in solid and dash-dotted lines, respectively.

follow the Vogel–Fulcher–Tammann (VFT) equation given by:

$$\tau_\alpha(T) = \tau_0 \exp\left(\frac{D_T T_0}{T - T_0}\right) \quad (1)$$

where D_T is a measure of the fragility ($m = 134 \pm 2$) of the analysed relaxation process, τ_0 is a pre-exponential factor and T_0 is the Vogel temperature. By assuming $\tau_\alpha(T_g) = 100$ s the glass transition temperature of D- and L-fucose can be estimated to be

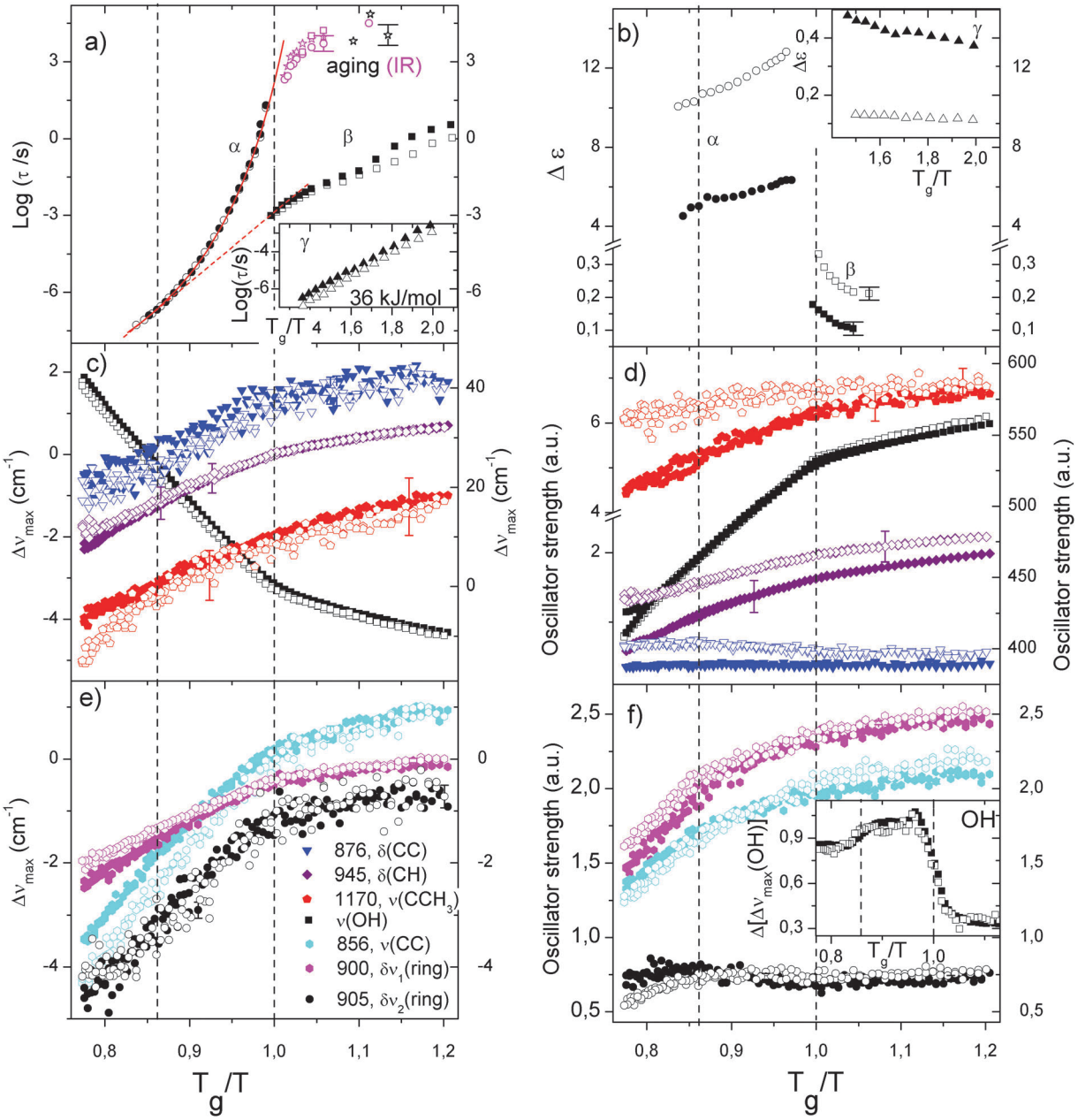

Fig. 3 (a) Dielectric relaxation time, τ, *vs.* T_g/T for L-fucose; in the insets in a and b the γ-relaxation is displayed. The relaxation times of α and β relaxations are depicted as black circles and squares, respectively, for L- (hollow) and D-fucose (solid). The solid red line shows the corresponding fit of the VFT dependence (eqn (1)) and the dashed red line shows the extrapolation of the β relaxation to high temperatures. Magenta coloured circles and stars refer to the aging time, determined from the spectral position and oscillator strength of the ν(OH) vibration, whereas hollow magenta squares are determined from the spectral position of δ_2(CH) upon aging. Aging time scales from BDS, τ_{ag}, are shown as black stars. (b) Relaxation strength of the dielectric relaxation processes *vs.* T_g/T; spectral shift, $\Delta\nu_{max}$, (c, e) and oscillator strength (d, f) of the chosen FTIR bands *vs.* T_g/T; the black squares, indicating the ν(OH) vibration, refer to the right *y*-axes, while all others refer to the left axes. The inset in f shows the variation of the spectral position of ν(OH) upon temperature steps of 2 K: $\Delta[\Delta\nu_{max}(OH)] = \Delta\nu_{max}(OH,T + 2K) - \Delta\nu_{max}(OH,T)$ *vs.* T_g/T. Vertical dashed lines (at $T_g/T = 0.86$ and 1) are a guide for the eye. All charts contain data measured upon heating and cooling.

306 K and 304 K, respectively. These values are comparable to T_g's of other six-carbon monosaccharides,[26] *e.g.* D-glucose (T_g = 308 K), galactose (T_g = 300 K) sorbose (T_g = 293 K) or fructose (T_g = 289 K). The relaxation rates of secondary processes (τ_β, τ_γ) are described for low temperatures by the Arrhenius equation written as:

$$\tau(T) = \tau_0 \exp(E_a/k_B T) \quad (2)$$

where k_B is the Boltzmann constant. The activation energy, E_a, is found to be independent of chirality (*i.e.* equal in L and D form), in particular E_a = 80 kJ mol^{-1} and E_a = 38 kJ mol^{-1} for the β and γ processes, respectively. Similar activation barriers for the β relaxation process in monosaccharides have been reported previously,[46] in our case $E_a(\gamma)$ seems to be smaller compared to other saccharides such as glucose, galactose or

fructose (E_a = 42 kJ mol^{-1}). This may be explained by a change in the H-bonding network resulting from the lower number of hydroxyl groups in fucose (4 OH groups) with respect to the other mentioned substances (5 OH groups). The qualitative behaviour of the dielectric strength ($\Delta\varepsilon$) of the three accessible dielectric relaxations, as shown in Fig. 3b is the same in D- and L-fucose. But there is a quantitative difference of roughly a factor of 2 that stems from the larger overall dipole moment of L- compared to D-fucose. In particular, dipole moments of μ = 4.7 D, 5.6 D, 1.6 D and 3.3 D for α-L-fucopyranose, α-L-fucofuranose, β-L-fucopyranose and β-L-fucofuranose, respectively, are calculated, whereas the same tautomers of D-fucose exhibit μ = 2.3 D, 3.3 D, 0.8 D and 1 D. In both, D- and L-fucose, the dielectric strength of the α and γ relaxation depends approximately linearly on inverse temperature. For $T_g/T > 1.05$ this also seems to be the case for the β process that shows a strong, gradual increase in $\Delta\varepsilon$ as T approaches the glass transition temperature. The observed decrease in $\Delta\varepsilon$ of the secondary relaxations when lowering temperature is well known and ascribed to reduced density fluctuations that govern the amplitude of these motions.[51] On the other hand, a drop in temperature increases the density of the sample, which enhances the dielectric strength of the α process as is observed for many glass forming liquids. Unfortunately, closer to T_g the α and β processes overlap strongly, resulting in an increased uncertainty of $\Delta\varepsilon$ and to a lesser extent in $\tau_{\alpha/\beta}$.

The spectral positions and oscillator strengths of the selected IR active vibrations are obtained by fitting combinations of pseudo Voigt functions to the FTIR data after subtracting a linear baseline.[17,19,52] This gives excellent agreement for all analysed bands except for the case of the OH stretching band (ν(OH)). This vibration is strongly asymmetrically broadened, most probably due to the presence of different types of hydrogen bonds (H-bonds) with varying binding energy, as described in the literature for different low and high molecular weight materials.[18,53–55] The average binding energy, E_{OHO}, of such H-bonds was empirically correlated with the difference of the spectral position ν_{max} of ν(OH) in the H-bonded and free (non H-bonded) state.[56,57] Hence, considering the temperature dependence of the ν(OH) vibration (*cf.* Fig. 2e and 3c) the binding energy varies from about −23 to −19 kJ mol^{-1} upon heating from 253 to 353 K. These energies compare well with the binding energy of the OH···O bridge as determined from DFT calculations for a CH_3OH···fucose interaction. We are not able to reliably deconvolve the peak into several contributions, since a clear indication of more than one peak could not be found neither in the second derivative nor in difference spectra. To overcome that and extract quantitative information anyway, we decided to approximate that band with an asymmetric pseudo Voigt function, as proposed by Stancik and Brauns.[58]

The temperature dependencies of the results of all analysed vibrational absorptions are combined in Fig. 3c–f. Oscillator strength of almost each band analysed here increases with decreasing temperature as an effect of an increased contrast on the occupation number and in the case of ν(OH) also because of an increased probability of H-bonding. Similarly, an increase of ν_{max} is found with decreasing T for all bands (except ν(OH)), which is attributed to thermal contraction resulting in a strengthening of the bond and, hence, its vibrational frequency. In the case of ν(OH) the aforementioned effect is suppressed by a dramatic increase of probability and strength of hydrogen bonding that weakens the O–H bond by pulling away the hydrogen atom.[18]

Analysing these dependencies in more detail, we find the OH stretching band at about 3400 cm^{-1} to be sensitive to the dynamic glass transition in its spectral position and oscillator strength. This can be seen in the sharp change in the slope of ν_{max} and f_{ij} (when plotted *versus* (*vs.*) T or T^{-1}) that originates from an accelerated formation of stronger H-bonds above T_g. The observed change in H-bonding may be the reason or the result of the macroscopic densification. Similar findings have been reported in the literature for other substances, all fitting into the picture of inter-molecular association driven by polar (electrostatic) interactions as an important factor of vitrification.[32,52,59,60] Especially the correlation of T_g (∼305 K) and ν_{max} (∼3370 cm^{-1}) of the ν(OH) band as found by Imamura *et al.* for systems with five OH groups per ring is reproduced here.[32] Several IR active moieties exhibit a kink in the temperature dependencies of their spectral positions around T_g. These include major contributions of the following type (*cf.* Table 1): CC ring stretching (at 856 cm^{-1}, named ν(CC)), CH deformation (δ(CH) at 876 cm^{-1}), combinations of CCO ring stretching and CH deformation modes ($\delta\nu_1$(ring) at 900 cm^{-1} and $\delta\nu_2$(ring) at 905 cm^{-1}) as well as a CH deformation (δ(CH) at 945 cm^{-1}). All of these bands are linked to the conformation of the ring. There is no such direct relation for the combination band at 1170 cm^{-1} (called $\nu(CCH_3)$ in the following), which exhibits major contributions from a C–CH_3 stretching motion and minor parts from CH_3 deformation. Consequently, we do not observe a kink here.

Plotting f_{ij} *vs.* T_g/T displays such pronounced changes in the slope at T_g only for ν(OH). All other analysed vibrations show a constant or a continuously varying slope for $f_{ij}(T_g/T)$ at this temperature. Surprisingly, a kink is observed for f_{ij} of ν(CC), $\delta\nu_1$(ring) and a weak one for $\delta\nu_2$(ring) well within the liquid state at $T_g/T \sim 0.86$ (T = 354 K = 1.16T_g). These 3 vibrations extend over the whole sugar ring and, hence, are sensitive to the intra-molecular structure. For example, ν(CC) vanishes after transformation from chair to boat conformation of α-D-fucose according to the DFT calculations. Furthermore, we find a weak change in the slope of $\nu_{max}(T)$ of ν(OH) here (inset in Fig. 3f). Similar dependencies at a ratio of $T_g/T = 0.85 \pm 0.05$ have been reported for the carbonyl stretching band in citrates[18] and salol[16,17] indicating changes in the intra-molecular mobility. This temperature ratio resembles for fucose and the other two cases the point where the high temperature extrapolation of a secondary relaxation time matches τ_α, *i.e.* the point where structural and secondary processes merge. Changes in structural dynamics of various glass formers have been observed in that temperature range in several other studies.[61] Novikov and Sokolov discussed it in terms of a particle that is trapped in a cage and can escape if the thermal fluctuations of the cage are large enough. They argue that this should happen at a "universal" α relaxation time of about 10^{-6} s to 10^{-8} s,[61] which agrees with the

τ_α at $T_g/T \sim 0.86$ found here. In citrates the mentioned temperature is linked to the point where the γ and α relaxation decouple, which is at $\tau_\alpha \sim 10^{-7}$ s, whereas in salol we find the merging point of β and α at that characteristic temperature ratio, being at $\tau_\alpha \sim 10^{-2}$ s.[17,18] So both examples contradict the explanation proposed by Novikov and Sokolov and indicate a more specific origin of the observed $\alpha\beta$ coupling. Here, for the case of fucose, we propose a molecular interpretation based on polar interactions of CH and OH groups. The importance of such CH···OH interactions has been proven experimentally for a wide range of carbohydrate crystals by Steiner and Saenger[62] and the corresponding interaction energies, E_{CHO}, are subject of numerous computational studies.[63–68] In particular, for the $CH_4\cdots OH_2$ contact $E_{CHO} \approx -2.9$ kJ mol^{-1} is found by Ornstein and Zheng.[68] Other authors got smaller values depending on the details of the calculations (*e.g.* $E_{CHO} \approx -2.2$ kJ mol^{-1} (ref. 66)), but certainly E_{CHO} is increased by electronegative substituents. For $OHCH_2CH_3\cdots OH_2$ contacts, E_{CHO} of approximately -3.1 kJ mol^{-1} was reported by Novoa and Mota.[67] These energies coincide with thermal energy at the extrapolated β α merging point being $k_BT = k_B\,1.16T_g = -2.9$ kJ mol^{-1}, where we observe a weak kink of ν_{max} of ν(OH) (Fig. 3f). Therefore, we conclude that the dynamic barriers between structural substates are strengthened by the enhanced H-bonding network below 354 K = $1.16T_g$, in contrast to the dynamic barriers of conformational fluctuations (β) that remain essentially unchanged. This is why we observe the splitting of the two relaxations, and the reduced changes in f_{ij} of conformationally sensitive bands below $1.16T_g$ (Fig. 3).

3.3 Aging dynamics

Besides the inter- and intra-molecular dynamics of L- and D-fucose depending on temperature, the impact of physical aging is investigated. BDS spectra reveal a decrease in dielectric loss of the β and γ processes with time (Fig. 4a). This is a universal scenario for secondary relaxation processes in glass forming liquids, and is commonly attributed to a decrease of the average angle of reorientation or the number of reorienting dipoles.[69–71] Furthermore, changes in the dielectric spectra at low frequencies are observed being explained by the slowing down of the structural relaxation process. In contrast to that, no shift of the relaxation times of both secondary modes can be observed as aging proceeds (Fig. 4a). This means that time aging-time superposition is not fulfilled. This is in contrast to previous aging measurements on different H-bonded systems.[72,73] Here we apply an approach proposed by Casalini and Roland,[74,75] to quantify the observed changes and estimate structural relaxation times in the glassy state, called "isostructural relaxation times". We adopt this term of the aforementioned study, although the shift of the α relaxation indicates structural evolution upon aging. The time dependence of the dielectric loss, ε'', measured at fixed frequencies, f_c, close to the maximum of the β and γ relaxation processes are fitted by the following equation derived by Leheny and Nagel (Fig. 4b).[76]

$$\varepsilon''(f_c, t_{ag}) = \Delta\varepsilon''(f_c)\exp\left[-\left(\frac{t_{ag}}{\tau_{ag}}\right)^{\beta_{ag}}\right] + \varepsilon_{eq}''(f_c) \qquad (3)$$

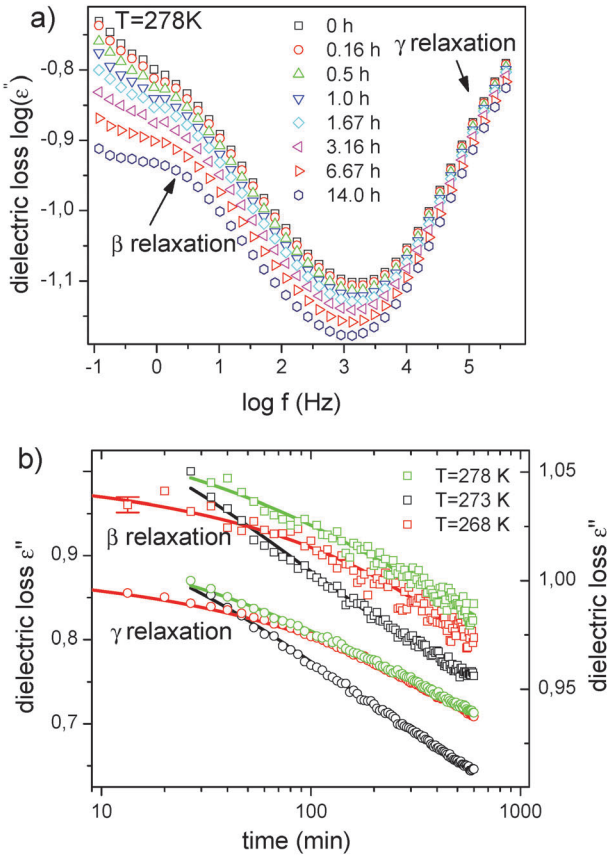

Fig. 4 (a) Dielectric loss spectra measured during physical aging of L-fucose at T = 278 K; (b) temporal evolution of dielectric loss at 10 Hz and 160 kHz, Squares refer to the β process (left axis), whereas circles to the γ process (right axis). Solid lines are fits according to a stretched exponential function with a β_{KWW} = 0.5.

where $\varepsilon_{eq}''(f_c) = \varepsilon(f_c, t_{ag} \to \infty)$ is the equilibrium value of ε'' and $\Delta\varepsilon''(f_c) = \varepsilon''(f_c, t_{ag} = 0) - \varepsilon_{eq}''(f_c)$ is the change in ε'' during aging. τ_{ag}, the aging time constant, is identified with the isostructural relaxation time. β_{ag} is the stretching exponent that does not vary significantly with temperature and is assumed to be equal to

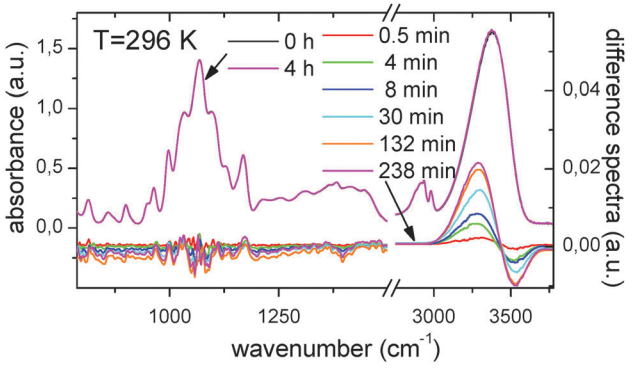

Fig. 5 Infrared spectra measured at the beginning and end (after 4 h) of physical aging of L-fucose at 296 K in black and magenta; the lower charts are difference spectra with respect to the initial state (t = 0 h) and refer to the right y axis, which is expanded by a factor of 35.

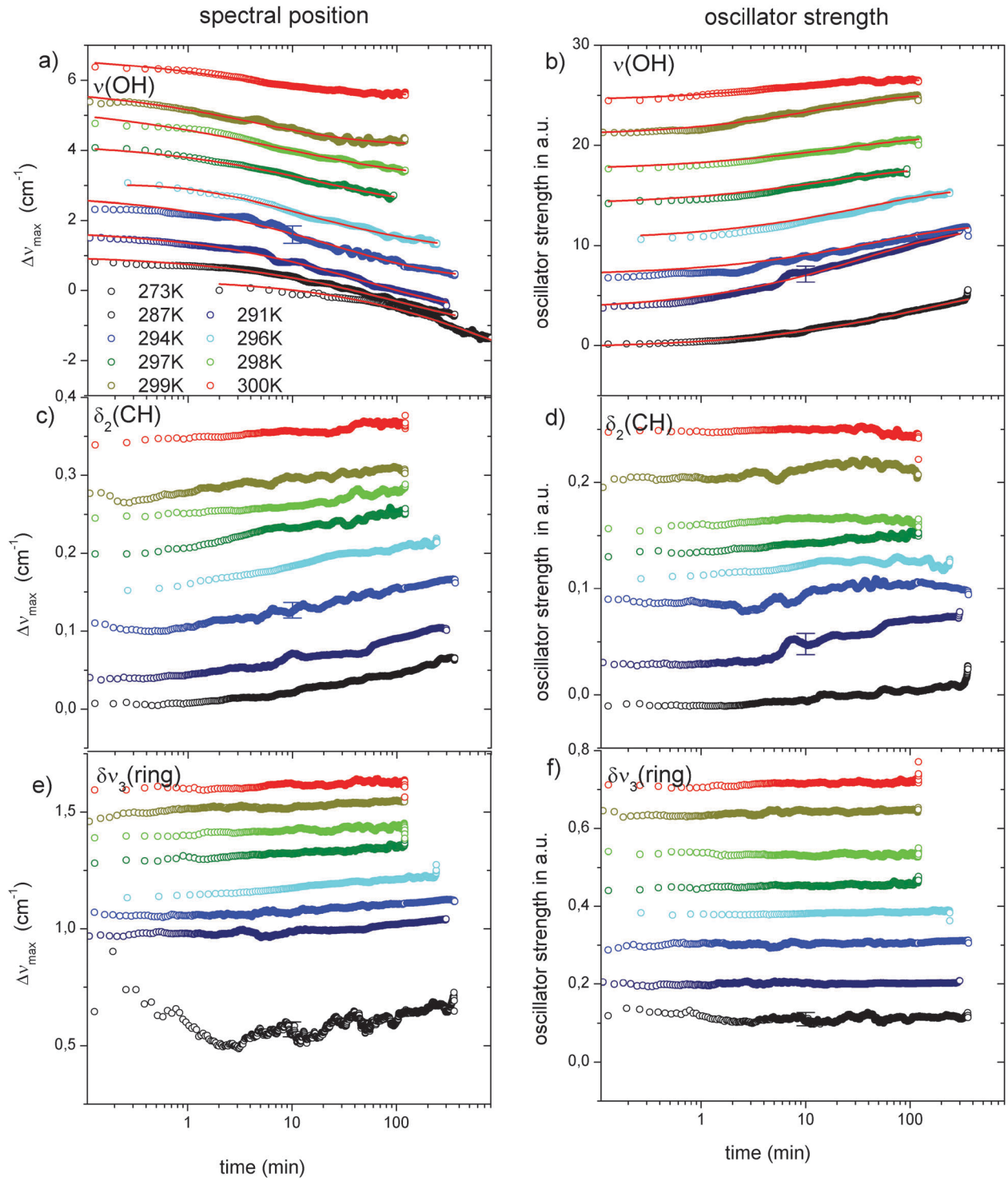

Fig. 6 Shift of the spectral position and oscillator strength *vs.* aging time for different vibrational modes as indicated. For the ν(OH) vibration (a, b) fits using a stretched exponential function are displayed as red lines (β_{IR} = 0.42).

β_{KWW}, as obtained from fitting the Kohlrausch–Williams–Watt (KWW) function to the structural loss peak measured just above T_g.[45,74] In the case of L-fucose $\beta_{ag} = \beta_{KWW} = 0.5$ is used as a fixed parameter during fitting.

The isostructural relaxation times, τ_{ag}, obtained from the slow and fast secondary relaxation processes agree and are shown in Fig. 3a. That there is no frequency dependence of τ_{ag} (*cf.* Fig. 4b) has been reported before for similar sugars well below T_g.[45] So there is only a single mechanism governing the rate exchange during aging.[77] Furthermore, we have to mention that the time scale of mutarotation is at least 2 orders of magnitude larger than τ_{ag} and, hence, there should be no

influence of it. Unfortunately, the results of τ_{ag} are somehow scattered, but change by less than an order of magnitude within the analysed temperature interval of 15 K.[26,78,79] The application of different analysis methods, *e.g.* as proposed by Lunkenheimer *et al.*,[72,73]‡ does not lead to systematically different results.

Studying physical aging by FTIR spectroscopy yields small, but significant, changes in the obtained spectra. This is exemplified in Fig. 5, where differences between the spectra at the beginning and end (t = 4 h) of the experiment are barely visible with the naked eye, but become obvious when magnified difference spectra are analysed. Especially for the ν(OH) band a clear red shift of ν_{max} and an asymmetric increase in f_{ij} can be observed as well as smaller changes within the fingerprint region. By application of the fitting procedure, as described above for the temperature dependent measurements, these subtle changes are quantified. Bands exhibiting a reasonably large variation in ν_{max} or f_{ij} (Fig. 5) are fitted with a stretched exponential function equivalent to eqn (3):

$$A(t_{IR}) = \Delta A \exp\left[-\left(\frac{t_{IR}}{\tau_{IR}}\right)^{\beta_{IR}}\right] + A_{eq}$$

$A(t_{IR})$ is the spectral position or oscillator strength at aging time t_{IR} or in thermal equilibrium (*i.e.* $A(t_{IR} \rightarrow \infty) = A_{eq}$). The stretching exponent, β_{IR}, is used as a shared parameter for all the dependencies of ν_{max} and f_{ij} on time and converged to a value of 0.46, which is remarkably close to the dielectric case (*cf.* Fig. 6). The extracted time constants, τ_{IR}, follow smooth and neither Arrhenius nor VFT like curves that, surprisingly, interlink the dielectrically determined structural, τ_α, and isostructural times, τ_{ag}, well (Fig. 3a). Such dependencies have been reported previously for different systems.[80–83] Moreover, τ_{IR} of ν(OH) coincides with the time constant from BDS at T = 273 K within experimental accuracy. This coincidence over such a wide temperature range indicates that τ_{ag} can be identified with τ_α below T_g at least in strongly H-bonding systems; and, furthermore, it underscores the role of the H-bonding network for the structure and the inter-molecular dynamics of L-fucose as reported for different systems by Gainaru *et al.*[84] and Preuß *et al.*[85] The IR aging times of δ_2(CH) appear to follow a steeper dependence than ν_{max} and f_{ij} of ν(OH) differing by a factor of up to 3. This significantly exceeds the experimental uncertainties. Unfortunately, only three rates can be extracted for δ_2(CH), which forbids further conclusions. But considering the sensitivity of δ_2(CH) to the intra-molecular structure, the observed differences between $\tau_{IR}(\nu(OH))$ and $\tau_{IR}(\delta_2(CH))$ are rationalized at least qualitatively. The significant difference, of up to a factor of 2, observed when comparing rates determined from oscillator strength and the spectral position of the ν(OH) band can be explained by the following: f_{ij} is proportional to the transition probability and the change in dipole moment when exciting ν(OH), whereas ν_{max} depends on the energy of the hydrogen bond amongst others. These 3 quantities vary differently with structural changes, *e.g.* with the changing distance of two hydroxyl groups.[17,56,57]

‡ Lunkenheimer *et al.* found frequency dependent aging rates in the vicinity of T_g, if they do not consider the aging rate as a function of aging time.

4 Conclusion

The inter- and intra-molecular dynamics of D- and L-fucose are studied in a wide range of temperatures below and above the calorimetric glass transition temperature T_g by combining dielectric and IR-spectroscopic measurements. For the different intra-molecular vibrations characteristic temperature dependencies of their spectral positions and oscillator strengths are found: while, for instance, the OH stretching vibration ν(OH) shows a pronounced kink at T_g, the $\nu(CCH_3)$ vibration does not perform any discontinuity at this temperature. Coupling of intra- and inter-molecular dynamics takes place at $T \sim 1.16T_g$ ($T_g/T \sim 0.86$), where the α relaxation merges with the extrapolated β relaxation. Here the OH stretching vibration shows a kink in the temperature dependence of the spectral position, and conformationally sensitive vibrations, like ν(CC), exhibit a change in the slope of the oscillator strength. This is explained by attractive CH$\cdots$O interactions that strengthen the H-bonding network and slow down the α relaxation with respect to conformational fluctuations (β). Physical aging below T_g, attributed solely to the equilibration of the H-bonding network, reveals a bending off of the aging dynamics from the equilibrium VFT dependence, indicating no divergence of the structural relaxation time. Furthermore, both stereoisomers show quite similar temperature dependencies in the BDS and FTIR experiments.

Acknowledgements

The authors like to thank ''Build-Mona – the Leipzig school of Natural Science''; Schsische Forschgruppe: FOR 877 ''From Local Constraints to Macroscopic Transport'' and the Deutsche Forschungsgemeinschaft (within the SFB-TRR 102) for financial support. K.K., S.P. and M.P. acknowledge financial support from the Polish National Science Centre on the basis of decision No. DEC-2012/05/B/ST4/00089. K.A. acknowledges financial assistance from National Centre for Research and Development (nanomaterials and their potential application in nanobiomedicine). The research was supported in part by PL-Grid Infrastructure.

References

1 R. Richert and A. Blumen, *Disorder Effects on Relaxational Processes: Glasses, Polymers, Proteins*, Springer, 1st edn, 1994.
2 P. G. DeBenedetti, *Metastable Liquids: Concepts and Principles*, Princeton University Press, 1996.
3 E. Donth, *The Glass Transition: Relaxation Dynamics in Liquids and Disordered Materials*, Springer, 2001.
4 C. A. Angell, *Science*, 1995, **267**, 1924–1935.
5 M. D. Ediger, C. A. Angell and S. R. Nagel, *J. Phys. Chem.*, 1996, **100**, 13200–13212.

6 S. Kahle, J. Gapinski, G. Hinze, A. Patkowski and G. Meier, *J. Chem. Phys.*, 2005, **122**, 074506.
7 G. R. Moran, K. R. Jeffrey, J. M. Thomas and J. R. Stevens, *Carbohydr. Res.*, 2000, **328**, 573–584.
8 S. Pawlus, S. Khodadadi and A. P. Sokolov, *Phys. Rev. Lett.*, 2008, **100**, 108103.
9 S. Khodadadi, S. Pawlus and A. P. Sokolov, *J. Phys. Chem. B*, 2008, **112**, 14273–14280.
10 G. Adam and J. H. Gibbs, *J. Chem. Phys.*, 1965, **43**, 139–146.
11 M. H. Cohen and D. Turnbull, *J. Chem. Phys.*, 1959, **31**, 1164–1169.
12 H. Sillescu, *J. Non-Cryst. Solids*, 1999, **243**, 81–108.
13 H. Tanaka, *J. Phys.: Condens. Matter*, 1999, **11**, L159–L168.
14 F. Qi, R. Böhmer and H. Sillescu, *Phys. Chem. Chem. Phys.*, 2001, **3**, 4022–4028.
15 F. Qi, G. Hinze, R. Böhmer, H. Sillescu and H. Zimmermann, *Chem. Phys. Lett.*, 2000, **328**, 257–262.
16 A. Döß, G. Hinze, R. Böhmer, H. Sillescu, H. Kolshorn, M. Vogel and H. Zimmermann, *J. Chem. Phys.*, 2000, **112**, 5884–5892.
17 P. Papadopoulos, W. Kossack and F. Kremer, *Soft Matter*, 2013, **9**, 1600–1603.
18 W. K. Kipnusu, W. Kossack, C. Iacob, P. Zeigermann, M. Jasiurkowska, J. R. Sangoro, R. Valiullin and F. Kremer, *Soft Matter*, 2013, **9**, 4681–4686.
19 W. K. Kipnusu, W. Kossack, C. Iacob, M. Jasiurkowska, J. Rume Sangoro and F. Kremer, *Z. Phys. Chem.*, 2012, **226**, 797–805.
20 D. J. Becker and J. B. Lowe, *Glycobiology*, 2003, **13**, 41R–53R.
21 F. Kremer and A. Schönhals, *Broadband dielectric spectroscopy*, Springer, 2003.
22 P. Griffiths and J. A. Haseth, *Fourier Transform Infrared Spectrometry*, Wiley-Interscience, 2nd edn, 2007.
23 K. Kaminski, P. Wlodarczyk, K. Adrjanowicz, E. Kaminska, Z. Wojnarowska and M. Paluch, *J. Phys. Chem. B*, 2010, **114**, 11272–11281.
24 P. Wlodarczyk, K. Kaminski, K. Adrjanowicz, Z. Wojnarowska, B. Czarnota, M. Paluch, J. Ziolo and J. Pilch, *J. Chem. Phys.*, 2009, **131**, 125103.
25 V. Molinero and W. A. Goddard, *Phys. Rev. Lett.*, 2005, **95**, 045701.
26 P. Wlodarczyk, K. Kaminski, M. Paluch and J. Ziolo, *J. Phys. Chem. B*, 2009, **113**, 4379–4383.
27 K. Kaminski, E. Kaminska, S. Pawlus, P. Wlodarczyk, M. Paluch, J. Ziolo, A. Kasprzycka, W. Szeja, K. L. Ngai and J. Pilch, *Carbohydr. Res.*, 2009, **344**, 2547–2553.
28 K. Kaminski, K. Adrjanowicz, E. Kaminska, K. Grzybowska, L. Hawelek, M. Paluch, M. Tarnacka, I. Gruszka and A. Kasprzycka, *Phys. Rev. E: Stat. Phys., Plasmas, Fluids, Relat. Interdiscip. Top.*, 2012, **86**, 031506.
29 K. Kaminski, K. Adrjanowicz, D. Zakowiecki, E. Kaminska, P. Wlodarczyk, M. Paluch, J. Pilch and M. Tarnacka, *Mol. Pharmaceutics*, 2012, **9**, 1559–1569.
30 K. Kaminski, P. Wlodarczyk and M. Paluch, *J. Chem. Phys.*, 2011, **135**, 167102.
31 H.-J. Kwon, J.-A. Seo, H. K. Kim and Y.-H. Hwang, *J. Chem. Phys.*, 2011, **134**, 014508.
32 K. Imamura, K. Sakaura, K.-i. Ohyama, A. Fukushima, H. Imanaka, T. Sakiyama and K. Nakanishi, *J. Phys. Chem. B*, 2006, **110**, 15094–15099.
33 W. F. Wolkers, A. E. Oliver, F. Tablin and J. H. Crowe, *Carbohydr. Res.*, 2004, **339**, 1077–1085.
34 W. Wolkers, A. Bochicchio, G. Selvaggi and F. A. Hoekstra, *Plant Physiol.*, 1998, **116**, 1169–1177.
35 M. J. Frisch, G. W. Trucks, H. B. Schlegel, G. E. Scuseria, M. A. Robb, J. R. Cheeseman, G. Scalmani, V. Barone, B. Mennucci, G. A. Petersson, H. Nakatsuji, M. Caricato, X. Li, H. P. Hratchian, A. F. Izmaylov, J. Bloino, G. Zheng, J. L. Sonnenberg, M. Hada, M. Ehara, K. Toyota, R. Fukuda, J. Hasegawa, M. Ishida, T. Nakajima, Y. Honda, O. Kitao, H. Nakai, T. Vreven, J. A. Montgomery Jr., J. E. Peralta, F. Ogliaro, M. Bearpark, J. J. Heyd, E. Brothers, K. N. Kudin, V. N. Staroverov, R. Kobayashi, J. Normand, K. Raghavachari, A. Rendell, J. C. Burant, S. S. Iyengar, J. Tomasi, M. Cossi, N. Rega, J. M. Millam, M. Klene, J. E. Knox, J. B. Cross, V. Bakken, C. Adamo, J. Jaramillo, R. Gomperts, R. E. Stratmann, O. Yazyev, A. J. Austin, R. Cammi, C. Pomelli, J. W. Ochterski, R. L. Martin, K. Morokuma, V. G. Zakrzewski, G. A. Voth, P. Salvador, J. J. Dannenberg, S. Dapprich, A. D. Daniels, Ö. Farkas, J. B. Foresman, J. V. Ortiz, J. Cioslowski and D. J. Fox, *Gaussian 09 Revision A.1*, Gaussian Inc., Wallingford CT, 2009.
36 T. Petrenko and F. Neese, *J. Chem. Phys.*, 2007, **127**, 164319.
37 W. J. Hehre, L. Radom, P. V. R. Schleyer and J. A. Pople, *Ab initio molecular orbital theory*, Wiley, New York, 1986.
38 R. G. Parr and W. Yang, *Density-functional theory of atoms and molecules*, Oxford University Press, Clarendon Press, New York, Oxford (GB), 1989.
39 K. Burke, J. P. Perdew and Y. Wang, *Electronic Density Functional Theory: Recent Progress and New Directions*, Springer, 1998.
40 A. D. Becke, *Phys. Rev. A*, 1988, **38**, 3098–3100.
41 A. D. Becke, *J. Chem. Phys.*, 1993, **98**, 5648–5652.
42 C. Lee, W. Yang and R. G. Parr, *Phys. Rev. B: Condens. Matter Mater. Phys.*, 1988, **37**, 785–789.
43 R. Krishnan, J. S. Binkley, R. Seeger and J. A. Pople, *J. Chem. Phys.*, 1980, **72**, 650–654.
44 D. J. Crofton and R. A. Pethrick, *Polymer*, 1981, **22**, 1048–1053.
45 K. Kaminski, K. Adrjanowicz, E. Kaminska and M. Paluch, *Phys. Rev. E: Stat. Phys., Plasmas, Fluids, Relat. Interdiscip. Top.*, 2011, **83**, 061502.
46 K. Kaminski, E. Kaminska, M. Paluch, J. Ziolo and K. L. Ngai, *J. Phys. Chem. B*, 2006, **110**, 25045–25049.
47 E. Säwén, PhD thesis, Department of Organic Chemistry, Stockholm University, Stockholm, 2011.
48 P. Wlodarczyk, K. Kaminski, S. Haracz, M. Dulski, M. Paluch, J. Ziolo and M. Wygledowska-Kania, *J. Chem. Phys.*, 2010, **132**, 195104.
49 P. Wlodarczyk, M. Paluch, L. Hawelek, K. Kaminski and J. Pionteck, *J. Chem. Phys.*, 2011, **134**, 175102.

50 S. Havriliak and S. Negami, *J. Polym. Sci., Part C: Polym. Symp.*, 1966, **14**, 99117.
51 K. L. Ngai and M. Paluch, *J. Chem. Phys.*, 2004, **120**, 857–873.
52 M. Jasiurkowska, W. Kossack, R. Ene, C. Iacob, W. K. Kipnusu, P. Papadopoulos, J. R. Sangoro, M. Massalska-Arod and F. Kremer, *Soft Matter*, 2012, **8**, 5194–5200.
53 A. Choperena and P. Painter, *Macromolecules*, 2011, **42**, 6159–6165.
54 B. T. Lutz and J. H. van der Maas, *J. Mol. Struct.*, 1997, **436–437**, 213–231.
55 K. Morokuma, *J. Chem. Phys.*, 1971, **55**, 1236–1244.
56 A. V. Iogansen, *Spectrochim. Acta, Part A*, 1999, **55**, 1585–1612.
57 G. R. Desiraju and T. Steiner, *The Weak Hydrogen Bond: In Structural Chemistry and Biology*, Oxford University Press, USA, 2001.
58 A. L. Stancik and E. B. Brauns, *Vib. Spectrosc.*, 2008, **47**, 66–69.
59 K. A. Masser, H. Zhao, P. C. Painter and J. Runt, *Macromolecules*, 2010, **43**, 9004–9013.
60 P. Atorngitjawat, R. J. Klein, A. G. McDermott, K. A. Masser, P. C. Painter and J. Runt, *Polymer*, 2009, **50**, 2424–2435.
61 V. N. Novikov and A. P. Sokolov, *Phys. Rev. E: Stat. Phys., Plasmas, Fluids, Relat. Interdiscip. Top.*, 2003, **67**, 031507.
62 T. Steiner and W. Saenger, *J. Am. Chem. Soc.*, 1992, **114**, 10146–10154.
63 Z. Latajka and S. Scheiner, *J. Comput. Chem.*, 1987, **8**, 674–682.
64 J. J. Novoa, B. Tarron, M.-H. Whangbo and J. M. Williams, *J. Chem. Phys.*, 1991, **95**, 5179–5186.
65 M. M. Szczesniak, G. Chalasinski, S. M. Cybulski and P. Cieplak, *J. Chem. Phys.*, 1993, **98**, 3078–3089.
66 T. van Mourik and F. van Duijneveldt, *THEOCHEM*, 1995, **341**, 63–73.
67 J. J. Novoa and F. Mota, *Chem. Phys. Lett.*, 1997, **266**, 23–30.
68 R. L. Ornstein and Y.-J. Zheng, *J. Biomol. Struct. Dyn.*, 1997, **14**, 657–665.
69 G. Power, J. K. Vij and G. P. Johari, *J. Chem. Phys.*, 2006, **124**, 074509.
70 N. B. Olsen, T. Christensen and J. C. Dyre, *Phys. Rev. E: Stat. Phys., Plasmas, Fluids, Relat. Interdiscip. Top.*, 2000, **62**, 4435–4438.
71 N. B. Olsen, *J. Non-Cryst. Solids*, 1998, **235–237**, 399–405.
72 P. Lunkenheimer, R. Wehn, U. Schneider and A. Loidl, *Phys. Rev. Lett.*, 2005, **95**, 055702.
73 P. Lunkenheimer, R. Wehn and A. Loidl, *J. Non-Cryst. Solids*, 2006, **352**, 4941–4945.
74 R. Casalini and C. M. Roland, *Phys. Rev. Lett.*, 2009, **102**, 035701.
75 R. Casalini and C. M. Roland, *J. Non-Cryst. Solids*, 2011, **357**, 282–285.
76 R. L. Leheny and S. R. Nagel, *Phys. Rev. B: Condens. Matter Mater. Phys.*, 1998, **57**, 5154–5162.
77 R. Richert, *Phys. Rev. Lett.*, 2010, **104**, 085702.
78 K. Adrjanowicz, M. Paluch and K. L. Ngai, *J. Phys.: Condens. Matter*, 2010, **22**, 125902.
79 K. Adrjanowicz, D. Zakowiecki, K. Kaminski, L. Hawelek, K. Grzybowska, M. Tarnacka, M. Paluch and K. Cal, *Mol. Pharmaceutics*, 2012, **9**, 1748–1763.
80 J. Zhao, S. L. Simon and G. B. McKenna, *Nat. Commun.*, 2013, **4**, 1783.
81 A. Dhinojwala, G. K. Wong and J. M. Torkelson, *J. Chem. Phys.*, 1994, **100**, 6046–6054.
82 K. Paeng, S. F. Swallen and M. D. Ediger, *J. Am. Chem. Soc.*, 2011, **133**, 8444–8447.
83 Y. Rharbi, F. Boué and Q. Nawaz, *Macromolecules*, 2013, DOI: 10.1021/ma401523n.
84 C. Gainaru, S. Kastner, F. Mayr, P. Lunkenheimer, S. Schildmann, H. J. Weber, W. Hiller, A. Loidl and R. Böhmer, *Phys. Rev. Lett.*, 2011, **107**, 118304.
85 M. Preuß, C. Gainaru, T. Hecksher, S. Bauer, J. C. Dyre, R. Richert and R. Böhmer, *J. Chem. Phys.*, 2012, **137**, 144502.

